

Casimir effect with rough metallic mirrors

Paulo A. Maia Neto

Instituto de Física, UFRJ, Caixa Postal 68528, 21945-970 Rio de Janeiro RJ, Brazil

Astrid Lambrecht and Serge Reynaud

Laboratoire Kastler Brossel, CNRS, ENS, UPMC case 74, Campus Jussieu, 75252 Paris, France

We calculate the second order roughness correction to the Casimir energy for two parallel metallic mirrors. Our results may also be applied to the plane-sphere geometry used in most experiments. The metallic mirrors are described by the plasma model, with arbitrary values for the plasma wavelength, the mirror separation and the roughness correlation length, with the roughness amplitude remaining the smallest length scale for perturbation theory to hold. From the analysis of the intracavity field fluctuations, we obtain the Casimir energy correction in terms of generalized reflection operators, which account for diffraction and polarization coupling in the scattering by the rough surfaces. We present simple analytical expressions for several limiting cases, as well as numerical results that allow for a reliable calculation of the roughness correction in real experiments. The correction is larger than the result of the Proximity Force Approximation, which is obtained from our theory as a limiting case (very smooth surfaces).

PACS numbers: 42.50.-p, 03.70.+k, 68.35.Ct

I. INTRODUCTION

The Casimir force of attraction between metallic mirrors [1] has been measured with high experimental precision over the last few years [2]. These new experiments allow for an accurate theory/experiment comparison [3], opening the way for the search for new weak forces with submillimetric ranges [4]. On the theoretical front, accurate results based on realistic models are sorely needed in order to match the desired levels of accuracy. Three important effects provide the main corrections to the ideal configuration considered by Casimir: non zero temperature [5], finite conductivity [6, 7] and roughness of the mirrors [8]-[11]. Temperature corrections are important when the distance L between the mirrors is above $1\mu\text{m}$, whereas finite conductivity and roughness provide the major corrections for the short distances (of the order of a few hundred nanometers) probed by most experiments.

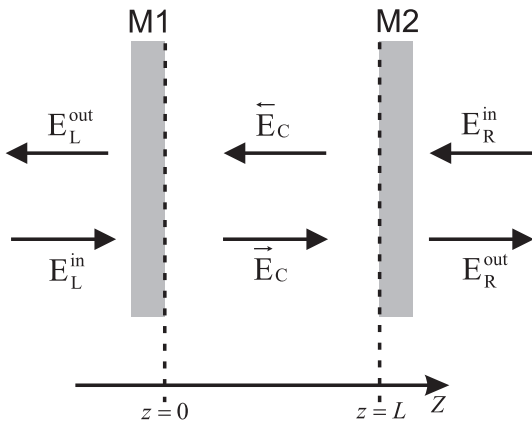
In principle, these effects must be taken into account simultaneously. The overall correction is not in general the product of the separate corrections calculated independently. In particular, the correlation between finite conductivity and roughness effects is essential, because they both intervene at the same range of L . Therefore, a reliable theory for short distances must analyze the roughness effect in the context of a finite-conductivity model for the material medium. To this aim, we describe the optical properties of the metallic mirrors by the plasma model.

When the surface profiles are nearly smooth over distances of the order of L , the roughness correction may be calculated from the Proximity Force Approximation (PFA) [12]. In this approximation, the Casimir energy is computed from the formula for parallel planes by averaging the ‘local’ distance over the surface [11]. In order to derive more general results, we develop a perturbative theory for the Casimir energy with rough plane mirrors,

allowing for the computation of the energy correction when the surface profile varies on arbitrarily short length scales, provided that they are larger than the roughness amplitude (otherwise the perturbative approximation would not apply). Our approach is applicable to most Casimir force measurements between metallic mirrors.

We follow the approach of Ref. [13], and consider the two mirrors as a plane Fabry-Perot cavity, which is treated as composed optical network in order to calculate the intracavity field fluctuations. We then derive a formal result for the Casimir energy up to second order in the amplitude of roughness, in terms of generalized reflection coefficients describing the scattering by rough surfaces, taking into account the coupling between Transverse Electric (TE) and Transverse Magnetic (TM) polarizations. Numerical results derived from the present calculation were presented in a letter [14], together with some analytical limiting cases. In this paper we present the complete derivation and the explicit formulas used in [14].

This paper is organized in the following way. In Sec. II, we present some basic definitions and assumptions, and discuss the validity of the PFA in two different contexts. In Sec. III, we derive the formal, general result for the second order roughness energy correction, which is then applied to the specific plasma-model calculation presented in Sec. IV. Several limiting cases are discussed in the following sections: the short roughness wavelength regime (Sec. V), the perfectly-reflecting limit (Sec. VI) and the plasmon limit (Sec. VII). In Sec. VIII, we discuss the example of a Gaussian roughness spectrum and present some concluding remarks. Three appendices present additional details of the derivations.

FIG. 1: Fabry-Perot cavity of length L .

II. GENERAL CONSIDERATIONS AND ASSUMPTIONS

Our Fabry-Perot cavity of length L is composed of two parallel mirrors with rough surfaces, as shown in Fig. 1. We analyze the cavity as a composed optical network, and calculate the fluctuations of the intracavity fields propagating along the positive and negative z -axis, \vec{E}_C and \overleftarrow{E}_C , in terms of the fluctuations of the incoming free-space fields E_L^{in} and E_R^{in} (also shown in Fig. 1 are the outgoing fields E_L^{out} and E_R^{out}). In appendix A, we show that the Casimir energy turns out to depend only on the coefficients describing the reflection of the intracavity fields by the internal sides of mirrors M1 and M2. The functions $h_1(\mathbf{r})$ and $h_2(\mathbf{r})$ define their surface profiles with respect to reference planes at $z = 0$ (see Fig. 2) and $z = L$, respectively. \mathbf{r} collects the two transverse coordinates (x, y) orthogonal to the cavity extension. By construction, both h_1 and h_2 have zero spatial averages: $\langle h_j \rangle = 0, j = 1, 2$, and are counted as positive when they correspond to local length decreases below the mean value L .

We assume that the two surfaces are statistically independent, so that the cross correlation function vanishes:

$$\langle h_1(\mathbf{r})h_2(\mathbf{r}') \rangle = 0. \quad (1)$$

Translational symmetry on the xy plane implies that the self correlation functions satisfy

$$\langle h_j(\mathbf{r})h_j(\mathbf{r}') \rangle = \langle h_j(\mathbf{r} - \mathbf{r}')h_j(\mathbf{0}) \rangle, \quad j = 1, 2.$$

Then in the Fourier domain we have (\mathbf{k} is a two-dimensional vector)

$$\langle H_j(\mathbf{k})H_j(\mathbf{k}') \rangle = (2\pi)^2 \delta^{(2)}(\mathbf{k} + \mathbf{k}') \sigma_{jj}(\mathbf{k}), \quad (2)$$

where $H_j(\mathbf{k})$ is the Fourier transformation of $h_j(\mathbf{r})$ and the roughness spectrum $\sigma_{jj}(\mathbf{k})$ is the Fourier transform of the self correlation function:

$$\sigma_{jj}(\mathbf{k}) = \int d^2\mathbf{r} e^{-i\mathbf{k}\cdot\mathbf{r}} \langle h_j(\mathbf{r})h_j(\mathbf{0}) \rangle.$$

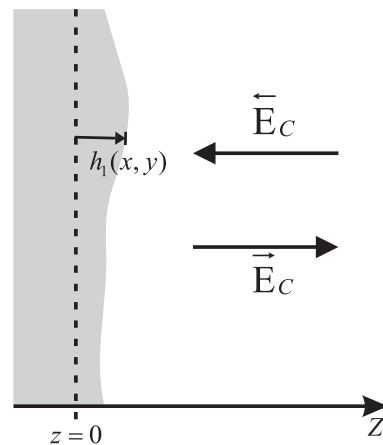


FIG. 2: Magnified detail of the internal surface of mirror M1.

We assume that the area A of the mirrors contains many correlation areas: $A \gg \ell_C^2$, where ℓ_C is the correlation length characteristic of the self correlation function. In this case, a single mirror already contains many independent realizations of surface profiles, and hence spatial and ensemble averages are equivalent.

We also assume that the deformation amplitudes are very small, in the scale of the mean cavity length, $|h_j| \ll L$, as well as in the scale of the correlation length, $|h_j| \ll \ell_C$, so that the surface profile gradients satisfy $|\nabla h_j| \ll 1$. This allows us to treat the surface deformations as small perturbations of the ideal plane geometry. The Casimir energy is then calculated up to second order of the deformation amplitudes. More precisely, the energy correction is obtained in terms of

$$\langle H_j(\mathbf{k})H_j(-\mathbf{k}) \rangle = A\sigma_{jj}(\mathbf{k}), \quad (3)$$

where we have used Eq. (2).

Most experiments are performed with a plane-sphere (PS) setup, instead of the plane-plane (PP) cavity used as the benchmark for our perturbative calculation. However, our results may also be applied to those experiments, provided that we use the PFA to connect the two different geometries. In this case, the force F_{PS} between a sphere of radius R and a plane at a distance of closest approach L is given in terms of the energy E_{PP} for the plane-plane cavity as follows:

$$F_{\text{PS}}(L) = 2\pi R \frac{E_{\text{PP}}(L)}{A} \quad (4)$$

The relative roughness correction of the force in the plane-sphere geometry may then be obtained from the relative energy correction calculated in this paper:

$$\Delta = \frac{\delta F_{\text{PS}}}{F_{\text{PS}}} = \frac{\delta E_{\text{PP}}}{E_{\text{PP}}}. \quad (5)$$

We emphasize that the PFA amounts to the addition of contributions corresponding to different local inter-plate

distances, assuming these contributions to be independent. But the Casimir energy is not additive, so that the PFA cannot be exact, although it is often improperly called a theorem.

Note that the conditions required for applying the PFA to connect the plane-sphere and the plane-plane geometries are quite different from those necessary for using the PFA in the computation of the roughness correction itself. In the first case, it is necessary that the radius R is large enough, so that the separation L satisfies $L \ll R$ [15]. Moreover, to avoid any interplay between curvature and roughness effects, one requires the correlation length ℓ_C to be small enough, so that many correlation areas are contained in a given nearly-plane local section of the spherical surface: $\ell_C^2 \ll RL$. In contrast, applying the PFA to roughness requires the surfaces to be nearly plane in the scale of the separation: $\ell_C \gg L$. Then, the following second-order roughness correction to the Casimir energy is obtained [11]:

$$\delta E_{\text{PP}} \approx \frac{E_{\text{PP}}''(L)}{2} \langle h_1^2 + h_2^2 \rangle, \quad (\text{PFA}) \quad (6)$$

Hence, the PFA result for the roughness correction depends on the second order derivative of the energy and on the variances of the length deformations h_1 and h_2 . This expression is equivalent to the procedure used for analyzing the effect of roughness in recent experiments [9, 16]. In the following sections, we will assume the PFA to provide a valid description of curvature, but not of roughness.

III. REFLECTION AND LOOP FUNCTIONS FOR ROUGH MIRRORS

In this section we start to develop a description of reflection by the internal sides of the cavity mirrors (see Fig. 1), leaving the more general theory which takes into account the coupling with the external fields to appendix A.

We take the mixed Fourier representation for the intracavity fields:

$$\vec{\mathbf{E}}_C(\mathbf{k}, z, \omega) = (\vec{\mathbf{E}}_C^{\text{TE}}(\mathbf{k}, \omega) \hat{\epsilon}^{\text{TE}} + \vec{\mathbf{E}}_C^{\text{TM}}(\mathbf{k}, \omega) \hat{\epsilon}^{\text{TM}}) e^{ik_z z}, \quad (7)$$

where ω is the frequency, \mathbf{k} is the two-dimensional wavevector associated to propagation parallel to the xy plane, and $k_z = \text{sgn}(\omega) \sqrt{\omega^2/c^2 - k^2}$, with sgn denoting the sign function. The complete wavevector is given by $\mathbf{K} = \mathbf{k} + k_z \hat{z}$. The field $\vec{\mathbf{E}}_C$ is written in a similar way, except for the replacement $k_z \rightarrow -k_z$. The TE and TM unitary vectors are defined in the following way:

$$\hat{\epsilon}^{\text{TE}} = \hat{z} \times \hat{k}, \quad (8)$$

$$\hat{\epsilon}^{\text{TM}} = \hat{\epsilon}^{\text{TE}} \times \hat{K}. \quad (9)$$

It is useful to employ the Dirac notation, with the ket $|\vec{\mathbf{E}}_C(\omega)\rangle$ providing a compact notation for the field amplitudes:

$$\vec{\mathbf{E}}_C^{\rightarrow p}(\mathbf{k}, \omega) = \langle \mathbf{k}, p | \vec{\mathbf{E}}_C(\omega) \rangle,$$

where $p = \text{TE}, \text{TM}$ denotes the polarization.

The reflection by the mirror M1 at frequency ω is written as

$$|\vec{\mathbf{E}}_C(\omega)\rangle = \mathcal{R}_1(\omega) |\overleftarrow{\mathbf{E}}_C(\omega)\rangle. \quad (10)$$

When the surface is rough, the operator $\mathcal{R}_1(\omega)$ mixes up different values of \mathbf{k} and polarizations. On the other hand, the field frequency is conserved, since the surface is at rest. The explicit form of (10) is

$$\vec{\mathbf{E}}_C^{\rightarrow p}(\mathbf{k}, \omega) = \int \frac{d^2 \mathbf{k}'}{(2\pi)^2} \sum_{p'} \langle \mathbf{k}, p | \mathcal{R}_1(\omega) | \mathbf{k}', p' \rangle \overleftarrow{\mathbf{E}}_C^{\leftarrow p'}(\mathbf{k}', \omega). \quad (11)$$

The reflection by mirror M2 is defined in a similar way in terms of the operator $\mathcal{R}_2(\omega)$.

We expand the reflection operators $\mathcal{R}_j(\omega)$, $j = 1, 2$, in powers of the deformation amplitudes h_j :

$$\mathcal{R}_j(\omega) = \mathcal{R}_j^{(0)}(\omega) + \delta \mathcal{R}_j^{(1)}(\omega) + \delta \mathcal{R}_j^{(2)}(\omega). \quad (12)$$

The zero-th order operators $\mathcal{R}_j^{(0)}$ correspond to ideally plane surfaces. They do not modify the polarization nor the momentum \mathbf{k} , and hence are diagonal in the basis $\{|\mathbf{k}, p\rangle\}$:

$$\langle \mathbf{k}, p | \mathcal{R}_j^{(0)}(\omega) | \mathbf{k}', p' \rangle = (2\pi)^2 \delta^{(2)}(\mathbf{k} - \mathbf{k}') \delta_{pp'} r_j^p(\mathbf{k}, \omega), \quad (13)$$

where $r_j^p(\mathbf{k}, \omega)$ are the specular reflection coefficients for a plane mirror.

For the ideal Fabry-Perot cavity, the Casimir effect may be entirely described by these reflection coefficients, which characterize the optical properties of the cavity as seen by the intracavity field [17]. As shown in Appendix A, a similar result holds for a cavity with rough mirrors, except that the specular reflection coefficients are replaced by the reflection operators defined above. The Casimir force is calculated from the spectral density characterizing the vacuum field fluctuations. For the intracavity field, the free-space spectral density for polarization p is multiplied by the generalized Airy function $g_p(\mathbf{k}, \omega)$, which quantifies the joint boundary effect of the two mirrors. We then derive the Casimir force after including the contribution of evanescent waves:

$$F_{\text{PP}} = A \sum_p \int \frac{d^2 k}{(2\pi)^2} \int_0^\infty \frac{d\omega}{2\pi} \hbar k_z (1 - g_p(\mathbf{k}, \omega)). \quad (14)$$

F_{PP} is defined as the z -component of the force on mirror M1; hence it is positive in case of attraction.

We compute $g_p(\mathbf{k}, \omega)$ up to second order in h_1 and h_2 :

$$g_p(\mathbf{k}, \omega) = g_p^{(0)}(\mathbf{k}, \omega) + \delta g_p^{(1)}(\mathbf{k}, \omega) + \delta g_p^{(2)}(\mathbf{k}, \omega). \quad (15)$$

$g_p^{(0)}(\mathbf{k}, \omega)$ is the Airy function for the ideal plane cavity [13]:

$$g_p^{(0)}(\mathbf{k}, \omega) = 1 + f_p(\mathbf{k}, \omega) + f_p(\mathbf{k}, \omega)^*,$$

where $f_p(\mathbf{k}, \omega)$ is the corresponding loop function. It is given by the superposition of all propagation factors representing a closed loop with n round-trips inside the cavity:

$$f_p(\mathbf{k}, \omega) = \sum_{n=1}^{\infty} (r_1^p(\mathbf{k}, \omega) r_2^p(\mathbf{k}, \omega) e^{-2\kappa L})^n = \frac{r_1^p(\mathbf{k}, \omega) r_2^p(\mathbf{k}, \omega) e^{-2\kappa L}}{1 - r_1^p(\mathbf{k}, \omega) r_2^p(\mathbf{k}, \omega) e^{-2\kappa L}}, \quad (16)$$

where $\kappa = -i\sqrt{\omega^2/c^2 - k^2}$. When replacing g_p by $g_p^{(0)}$ in (14), we find the well-known result for the Casimir force in the ideal case [17].

The first-order Casimir force correction, coming from $\delta g_p^{(1)}(\mathbf{k}, \omega)$ in (15), vanishes because it is proportional to the averages $\langle h_1 \rangle$ and $\langle h_2 \rangle$. Thus, the roughness correction is of second order, and results from the contribution of $\delta g_p^{(2)}(\mathbf{k}, \omega)$. These functions are written in terms of ‘rough’ loop functions $\delta f_p^{(2i)}(\mathbf{k}, \omega)$ and $\delta f_p^{(2ii)}(\mathbf{k}, \omega)$,

gathering the second-order contributions of the first ($\delta \mathcal{R}_j^{(1)}$) and second order ($\delta \mathcal{R}_j^{(2)}$) reflection operators, respectively:

$$\delta g_p^{(2)}(\mathbf{k}, \omega) = \delta f_p^{(2i)}(\mathbf{k}, \omega) + \delta f_p^{(2ii)}(\mathbf{k}, \omega) + c.c.. \quad (17)$$

$\delta f_p^{(2ii)}(\mathbf{k}, \omega)$ is the superposition of all closed loops involving a single second-order rough reflection at one of the mirrors:

$$\delta f_p^{(2ii)}(\mathbf{k}, \omega) = \frac{1}{A} \sum_{j=1}^2 \langle \mathbf{k}, p | \mathcal{D}(\omega)^{-1} e^{-\mathcal{K}(\omega)L} \mathcal{R}_{[j+1]}^{(0)}(\omega) e^{-\mathcal{K}(\omega)L} \delta \mathcal{R}_j^{(2)}(\omega) \mathcal{D}(\omega)^{-1} | \mathbf{k}, p \rangle, \quad (18)$$

with $[j+1]$ representing a sum modulo 2. Like $\mathcal{R}_j^{(0)}(\omega)$ in Eq. (13), the operators $\mathcal{D}(\omega)$ and $\mathcal{K}(\omega)$ are diagonal operators, with elements $1 - r_1^p(\mathbf{k}, \omega) r_2^p(\mathbf{k}, \omega) e^{-2\kappa L}$ and κ , respectively.

To understand why $\delta f_p^{(2ii)}(\mathbf{k}, \omega)$ is a generalization of the ideal loop function $f_p(\mathbf{k}, \omega)$, we should read the r.h.s. of Eq. (18) from right to left. The second-order rough reflection at mirror j is followed by a one-way propagation between the two mirrors (operator $\exp(-\mathcal{K}(\omega)L)$), and then by a specular reflection at mirror $[j+1]$. The loop is closed by a second one-way propagation back to mirror j . This loop can be preceded and/or followed by arbitrary numbers of round-trips with specular reflections, hence the entire expression is sandwiched between two operators $\mathcal{D}(\omega)^{-1}$.

‘Closing the loop’ means to ensure that the initial and final states are the same, which is represented by the ket $|\mathbf{k}, p\rangle$ and the corresponding bra in Eq. (18). Since all zero-th order processes conserve momentum and polarization, only second-order rough reflections that also conserve momentum and polarization are allowed, so that only *diagonal* elements of $\delta \mathcal{R}_j^{(2)}$ are expected to contribute in Eq. (18). Its explicit evaluation indeed yields [18]

$$\delta f_p^{(2ii)}(\mathbf{k}, \omega) = \frac{1}{A} \sum_{j=1}^2 \frac{r_{[j+1]}^p(\mathbf{k}, \omega) \langle \mathbf{k}, p | \delta \mathcal{R}_j^{(2)}(\omega) | \mathbf{k}, p \rangle e^{-2\kappa L}}{(1 - r_1^p(\mathbf{k}, \omega) r_2^p(\mathbf{k}, \omega) e^{-2\kappa L})^2}. \quad (19)$$

Those diagonal matrix elements are of the form

$$\langle \mathbf{k}, p | \delta \mathcal{R}_j^{(2)}(\omega) | \mathbf{k}, p \rangle = \int \frac{d^2 k'}{(2\pi)^2} R_{j;p}^{(2)}(\mathbf{k}, \mathbf{k}'; \omega) |H_j(\mathbf{k} - \mathbf{k}')|^2, \quad (20)$$

where the non-specular coefficients $R_{j;p}^{(2)}(\mathbf{k}, \mathbf{k}'; \omega)$ are in-

dependent of the profile functions $H_j(\mathbf{k})$.

On the other hand, nondiagonal matrix elements of $\delta\mathcal{R}_j^{(1)}$ contribute to the loop function $\delta f_p^{(2i)}(\mathbf{k}, \omega)$, because the latter contains two first-order rough reflections instead of just one second-order reflection. These elements are of the form

$$\langle \mathbf{k}, p | \delta\mathcal{R}_j^{(1)}(\omega) | \mathbf{k}', p' \rangle = R_{j;pp'}^{(1)}(\mathbf{k}, \mathbf{k}'; \omega) H_j(\mathbf{k} - \mathbf{k}'), \quad (21)$$

where again the coefficients $R_{j;pp'}^{(1)}(\mathbf{k}, \mathbf{k}'; \omega)$ are independent of $H_j(\mathbf{k})$. According to this expression, a given Fourier component $\Delta\mathbf{k}$ of the surface profile leads to a field momentum modification by $\Delta\mathbf{k}$.

Since the elements $\langle \mathbf{k}, p | \delta\mathcal{R}_j^{(1)}(\omega) | \mathbf{k}', p' \rangle$ are propor-

tional to $H_j(\mathbf{k} - \mathbf{k}')$, the terms associated to first-order rough reflections at *different* mirrors are proportional either to the product

$$H_1(\mathbf{k} - \mathbf{k}') H_2(\mathbf{k}' - \mathbf{k})$$

or to its complex conjugate. As discussed in Sec. II, we assume that their average values vanish because the two surface profiles are statistically independent. Thus, we only keep the terms associated to two first-order rough reflections at the same mirror when deriving $\delta f_p^{(2i)}(\mathbf{k}, \omega)$ (omitting the dependence with ω in the r.h.s.):

$$\delta f_p^{(2i)}(\mathbf{k}, \omega) = \frac{1}{A} \sum_{j=1}^2 \langle \mathbf{k}, p | \mathcal{D}^{-1} e^{-\kappa L} \mathcal{R}_{[j+1]}^{(0)} e^{-\kappa L} \delta\mathcal{R}_j^{(1)} \mathcal{D}^{-1} e^{-\kappa L} \mathcal{R}_{[j+1]}^{(0)} e^{-\kappa L} \delta\mathcal{R}_j^{(1)} \mathcal{D}^{-1} | \mathbf{k}, p \rangle. \quad (22)$$

As for Eq. (18), the sequence of events associated to these loops may be read from right to left in the r.h.s. of (22): first-order rough reflection by mirror j , one-way propagation to mirror $[j + 1]$, specular reflection, one-way back to j , second first-order rough reflection by j . To

restore the initial sense of propagation, the loop is closed by one or more specular round-trips. Before each rough reflection, arbitrary numbers of specular round-trips are allowed. Explicit evaluation yields

$$\delta f_p^{(2i)}(\mathbf{k}, \omega) = \frac{1}{A} \sum_{j=1}^2 \sum_{p'} \int \frac{d^2 k'}{(2\pi)^2} \frac{e^{-2(\kappa+\kappa')L} r_{j+1}^p(\mathbf{k}) r_{j+1}^{p'}(\mathbf{k}') \langle \mathbf{k}, p | \delta\mathcal{R}_j^{(1)}(\omega) | \mathbf{k}', p' \rangle \langle \mathbf{k}', p' | \delta\mathcal{R}_j^{(1)}(\omega) | \mathbf{k}, p \rangle}{(1 - r_1^p(\mathbf{k}, \omega) r_2^p(\mathbf{k}, \omega) e^{-2\kappa L})^2 (1 - r_1^{p'}(\mathbf{k}', \omega) r_2^{p'}(\mathbf{k}', \omega) e^{-2\kappa' L})}, \quad (23)$$

where $\kappa' = -i\sqrt{\omega^2/c^2 - k'^2}$.

Before replacing all these results into (14), we first write the Casimir force as the real part of integrals of the loop functions [13]. Since these functions are analytical, Cauchy theorem allows us to replace the integral over real frequencies by an integral over the imaginary axis in the complex plane of frequency. As a result, ω is replaced by $\xi = -i\omega$, and $\exp(-\kappa L)$ becomes a real

exponential factor, with

$$\kappa = \sqrt{k^2 + \frac{\xi^2}{c^2}} > 0.$$

The resulting integrals turn out to be real, and the roughness correction is then given by

$$\delta F_{\text{PP}}(L) = 2A \int \frac{d^2 k}{(2\pi)^2} \int_0^\infty \frac{d\xi}{2\pi} \hbar \kappa \sum_p \left[\delta f_p^{(2i)}(\mathbf{k}, \xi) + \delta f_p^{(2ii)}(\mathbf{k}, \xi) \right] \quad (24)$$

According to (19) and (20), $\delta f_p^{(2ii)}(\mathbf{k}, \xi)$ is given by an integral over \mathbf{k}' with the integrand proportional to $|H_j(\mathbf{k} - \mathbf{k}')|^2$. We also obtain this factor when computing

$\delta f_p^{(2i)}(\mathbf{k}, \xi)$ from (21) and (23). According to (3), when averaged it yields $A\sigma_{jj}(\mathbf{k} - \mathbf{k}')$, due to translational symmetry on the xy plane. Hence both loop functions are

independent of A , yielding a force proportional to A as expected.

The energy correction is computed from (24) by a simple integration:

$$\delta E_{\text{PP}}(L) = - \int_L^\infty \delta F_{\text{PP}}(L') dL'.$$

In order to simplify the notation, we consider two mirrors made of the same metal, and hence with the same optical properties (otherwise the correction is given by a trivial extension). Then, after transforming $\mathbf{k} - \mathbf{k}'$ into \mathbf{k} by a trivial change of integration variable and taking (3) into account, we find

$$\delta E_{\text{PP}} = \int \frac{d^2\mathbf{k}}{(2\pi)^2} G(\mathbf{k}) \sigma(\mathbf{k}), \quad (25)$$

$$b_{\mathbf{k}',\mathbf{k}''}^{(i)}(\xi) = \frac{1}{2} \sum_{p',p''} \frac{e^{-2(\kappa'+\kappa'')L} r^{p'}(\mathbf{k}',\xi) r^{p''}(\mathbf{k}'',\xi) R_{p',p''}^{(1)}(\xi;\mathbf{k}',\mathbf{k}'') R_{p'',p'}^{(1)}(\xi;\mathbf{k}'',\mathbf{k}')}{(1 - r^{p'}(\mathbf{k}',\xi)^2 e^{-2\kappa'L}) (1 - r^{p''}(\mathbf{k}'',\xi)^2 e^{-2\kappa'L})}, \quad (28)$$

whereas Eq. (19) leads to the following contribution from the second-order operator:

$$b_{\mathbf{k}',\mathbf{k}''}^{(ii)}(\xi) = \sum_p \frac{e^{-2\kappa'L} r^p(\mathbf{k}',\xi) R_p^{(2)}(\xi;\mathbf{k}',\mathbf{k}'')}{1 - r^p(\mathbf{k}',\xi)^2 e^{-2\kappa'L}}. \quad (29)$$

The response function $G(\mathbf{k})$ is entirely determined by the mirrors' non-specular coefficients $R_{pp}^{(1)}$ and $R_p^{(2)}$, together with the specular reflection coefficients and the exponential factors describing round-trip propagation inside the cavity. For isotropic material media, symmetry requires the response function to depend only on the modulus $k = |\mathbf{k}|$. According to (25), this k dependence describes the spectral sensitivity of the Casimir energy to roughness. Hence, in general the Casimir energy depends on the details of the roughness spectrum $\sigma(\mathbf{k})$, and not only on the roughness variance

$$\langle h_1^2 + h_2^2 \rangle = \int \frac{d^2\mathbf{k}}{(2\pi)^2} \sigma(\mathbf{k}).$$

When $G(k)$ is known and the roughness spectrum measured experimentally, Eq. (25) allows for a precise and straightforward calculation of the roughness correction to the Casimir force without using the proximity force approximation.

The PFA is recovered only when the the surface is very smooth, corresponding to a roughness spectrum $\sigma(\mathbf{k})$ sharply peaked around $\mathbf{k} = \mathbf{0}$. In this case, we may replace $G(k)$ by $G(0)$ in (25) to find

$$\delta E_{\text{PP}} \approx G(0) \langle h_1^2 + h_2^2 \rangle, \quad (\text{PFA}) \quad (30)$$

with $\sigma(\mathbf{k}) = \sigma_{11}(\mathbf{k}) + \sigma_{22}(\mathbf{k})$. As discussed in connection with Eq. (21), the \mathbf{k} in $G(\mathbf{k})$ represents the field momentum transfer induced by a given Fourier component of the surface profile. The second-order roughness response function $G(\mathbf{k})$ is given by the following general expression

$$G(\mathbf{k}) = -\hbar A \int_0^\infty \frac{d\xi}{2\pi} \int \frac{d^2\mathbf{k}'}{4\pi^2} b_{\mathbf{k}',\mathbf{k}-\mathbf{k}'} \quad (26)$$

$$b_{\mathbf{k}',\mathbf{k}''} = b_{\mathbf{k}',\mathbf{k}''}^{(i)}(\xi) + b_{\mathbf{k}',\mathbf{k}''}^{(ii)}(\xi). \quad (27)$$

The contribution of the first-order reflection operator is calculated from Eq. (23) (from now on we drop the index j indicating one of the two mirrors):

in agreement with Eq. (6) provided that the response function satisfies the limit

$$G(k \rightarrow 0) = \frac{E_{\text{PP}}''(L)}{2}, \quad (31)$$

with the Casimir energy in the ideal case given by [7]

$$E_{\text{PP}}(L) = \hbar A \int_0^\infty \frac{d\xi}{2\pi} \int \frac{d^2\mathbf{k}}{(2\pi)^2} \sum_p \ln(1 - r^p(\mathbf{k},\xi)^2 e^{-2\kappa L}). \quad (32)$$

As a consequence of general properties of the rough reflection coefficients at zero momentum transfer (specular limit), we show in appendix B that this limit is satisfied by any response function derived from (26) regardless of the model considered for the material medium.

IV. ROUGHNESS RESPONSE FUNCTION FOR THE PLASMA MODEL

In this section, we present an explicit computation of the response function $G(k)$, starting from the general result given by Eqs. (26)-(29), and taking the plasma model to describe the optical properties of the metallic mirrors. The dielectric function is given by

$$\epsilon = 1 + \frac{\omega_{\text{P}}^2}{\xi^2}.$$

The plasma wavenumber, wavelength and frequency are related by

$$k_{\text{P}} = \frac{2\pi}{\lambda_{\text{P}}} = \frac{\omega_{\text{P}}}{c}.$$

We also define

$$\kappa_t(\mathbf{k}, \xi) = \sqrt{\mathbf{k}^2 + \epsilon \frac{\xi^2}{c^2}} = \sqrt{\kappa^2 + k_p^2}$$

representing the imaginary part of the z component of the wavevector inside the metallic medium. The specular reflection coefficients are given by

$$r^{\text{TE}}(\mathbf{k}, \xi) = -\frac{\kappa_t - \kappa}{\kappa_t + \kappa}, \quad (33)$$

$$r^{\text{TM}}(\mathbf{k}, \xi) = \frac{\left(1 + \frac{\omega_p^2}{\xi^2}\right) \kappa - \kappa_t}{\left(1 + \frac{\omega_p^2}{\xi^2}\right) \kappa + \kappa_t}. \quad (34)$$

In order to compute the roughness reflection coefficients, we follow the perturbation approach of Ref. [19], which is based on the extinction theorem [20] and the Rayleigh hypothesis. The incident, reflected and transmitted fields are related by two integral equations, which are solved up to second order of $H_j(\mathbf{k})$ for the reflected field in terms of the incident field. This allows us to derive the non-specular coefficients $R_{pp'}^{(1)}(\mathbf{k}, \mathbf{k}'; \xi)$ and $R_p^{(2)}(\mathbf{k}, \mathbf{k}; \xi)$ defining the relevant matrix elements of the first and second-order reflection operators.

However, it turns out to be simpler to first calculate the coefficients $\Lambda_{pp'}^{(1)}(\xi; \mathbf{k}, \mathbf{k}')$ defined as follows:

$$R_{pp'}^{(1)}(\mathbf{k}, \mathbf{k}'; \xi) = \frac{r^p(\mathbf{k}, \xi) t^{p'}(\mathbf{k}', \xi)}{t^p(\mathbf{k}, \xi)} \Lambda_{pp'}^{(1)}(\xi; \mathbf{k}, \mathbf{k}'), \quad (35)$$

where $t^p(\mathbf{k}, \xi)$ are the transmission coefficients for the plane interface (see Appendix A).

For given values of \mathbf{k} and \mathbf{k}' , we cast the four coefficients $\Lambda_{pp'}^{(1)}(\xi; \mathbf{k}, \mathbf{k}')$ into the 2×2 matrix $\Lambda^{(1)}(\mathbf{k}, \mathbf{k}')$ (with the association TE = 1, TM = 2), whose nondiagonal elements represent the coupling between TE and TM polarizations. We find

$$\Lambda^{(1)}(\mathbf{k}, \mathbf{k}') = \Lambda_-^{(1)}(\mathbf{k}, \mathbf{k}') - \Lambda_+^{(1)}(\mathbf{k}, \mathbf{k}'),$$

$$\Lambda_{\pm}^{(1)}(\mathbf{k}, \mathbf{k}') = (\kappa_t \pm \kappa) \mathbf{B}_t^{-1} \begin{pmatrix} C & S \\ -\frac{S}{1 \pm \beta \beta_t} & \frac{C \pm \beta \beta_t'}{1 \pm \beta \beta_t} \end{pmatrix} \mathbf{B}'_t, \quad (36)$$

$C = \mathbf{k} \cdot \mathbf{k}' / (k k')$ and $S = \sqrt{1 - C^2}$. We have also defined

$$\beta = \frac{k}{\kappa} \quad \beta_t = \frac{k}{\kappa_t}$$

$$\mathbf{B}_t = \begin{pmatrix} 1 & 0 \\ 0 & \frac{c \kappa_t}{\sqrt{\epsilon} \xi} \end{pmatrix}.$$

Primed quantities are likewise defined in terms of \mathbf{k}' .

The second-order coefficients are written in a similar way, with

$$R_p^{(2)}(\mathbf{k}, \mathbf{k}'; \xi) = r^p(\mathbf{k}, \xi) \Lambda_p^{(2)}(\xi; \mathbf{k}, \mathbf{k}'). \quad (37)$$

$\Lambda_{\text{TE}}^{(2)}(\xi; \mathbf{k}, \mathbf{k}')$ and $\Lambda_{\text{TM}}^{(2)}(\xi; \mathbf{k}, \mathbf{k}')$ are the diagonal elements of the matrix

$$\Lambda^{(2)}(\mathbf{k}, \mathbf{k}') = 2\kappa \kappa_t \mathbf{I} - \Lambda^{(1)}(\mathbf{k}, \mathbf{k}') \Lambda_-^{(1)}(\mathbf{k}, \mathbf{k}') \quad (38)$$

with \mathbf{I} denoting the 2×2 identity matrix.

By replacing these results into (28) and (29), we find the explicit expressions for the functions $b_{\mathbf{k}, \mathbf{k}'}^{(i)}(\xi)$ and $b_{\mathbf{k}, \mathbf{k}'}^{(ii)}(\xi)$:

$$b_{\mathbf{k}, \mathbf{k}'}^{(i)}(\xi) = \frac{1}{2} \sum_{\epsilon, \epsilon' = +, -} \mu_{\epsilon} \mu'_{\epsilon'} \left[f_{\text{TE}}(\mathbf{k}, \xi) f_{\text{TE}}(\mathbf{k}', \xi) C^2 (1 + \epsilon \beta \beta_t) (1 + \epsilon' \beta' \beta_t') + f_{\text{TE}}(\mathbf{k}, \xi) f_{\text{TM}}(\mathbf{k}', \xi) S^2 (1 + \epsilon \beta \beta_t) \right. \\ \left. + f_{\text{TM}}(\mathbf{k}, \xi) f_{\text{TE}}(\mathbf{k}', \xi) S^2 (1 + \epsilon' \beta' \beta_t') + f_{\text{TM}}(\mathbf{k}, \xi) f_{\text{TM}}(\mathbf{k}', \xi) (C + \epsilon \beta \beta_t') (C + \epsilon' \beta' \beta_t) \right], \quad (39)$$

$$b_{\mathbf{k}, \mathbf{k}'}^{(ii)}(\xi) = 2\kappa_t \kappa (f_{\text{TE}}(\mathbf{k}, \xi) + f_{\text{TM}}(\mathbf{k}, \xi)) + \sum_{\epsilon = +, -} \mu_{\epsilon} \mu'_{\epsilon} \left[f_{\text{TE}}(\mathbf{k}, \xi) (1 - C^2 \beta' \beta_t') (1 + \epsilon \beta \beta_t) \right. \\ \left. + f_{\text{TM}}(\mathbf{k}, \xi) S^2 (1 - \beta' \beta_t') + f_{\text{TM}}(\mathbf{k}, \xi) (C + \epsilon \beta \beta_t') (C - \beta' \beta_t) \right], \quad (40)$$

with

$$\mu_{\pm} = \frac{\kappa \pm \kappa_t}{1 \pm \beta \beta_t}.$$

These expressions can now be applied to the numerical computation of the response function for arbitrary values of L and λ_P . In Fig. 3, we plot G/E_{PP} as a function of

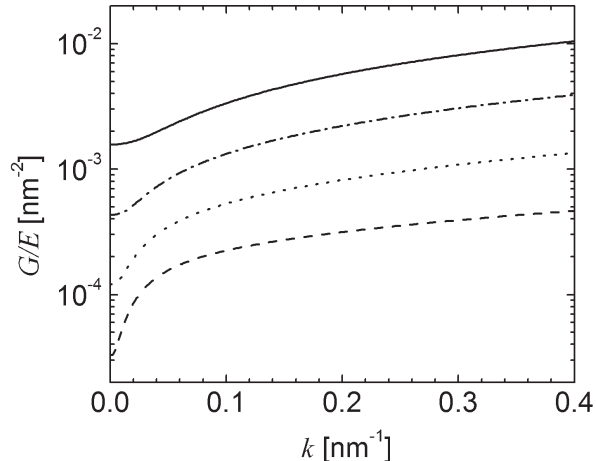


FIG. 3: Variation of G/E_{PP} versus k for the distances $L = 50\text{nm}$ (solid line), $L = 100\text{nm}$ (dashed-dotted line), $L = 200\text{nm}$ (dotted line), and $L = 400\text{nm}$ (dashed line). We take $\lambda_{\text{P}} = 136\text{nm}$.

k for several different values of the distance L , and for $\lambda_{\text{P}} = 136\text{nm}$, which corresponds to gold covered mirrors.

According to (25), this ratio provides the relative correction of the Casimir energy in the plane-plane configuration when integrated over the roughness spectrum $\sigma(\mathbf{k})$. Moreover, from (5) it also provides the relative force correction Δ for the plane-sphere geometry when the sphere radius is sufficiently large. Fig. 3 indicates that the relative correction is larger for shorter distances.

The behavior of $G(k)$ as $k \rightarrow 0$ is related to the PFA, and was already discussed in connection with Eq. (31). In addition to the verification of the general $G(k)$ given by (26)-(29) (see Appendix B), we have also verified independently that the explicit result derived from (39) and (40) also agrees with Eq. (31).

The fact that G increases as k grows from zero, as displayed in Fig. 3, implies that the PFA underestimates the roughness correction. In order to quantify the departure from the PFA description, we define the sensitivity function

$$\rho(k) = \frac{G(k)}{G(0)}. \quad (41)$$

In Fig. 4, we plot ρ as function of k for the same values of distance and λ_{P} employed in Fig. 3. The PFA amounts to replace $\rho(k)$ by unity for all values of k contained in the roughness spectrum $\sigma(k)$. Clearly, this approximation is better for shorter distances, and smaller values of k (corresponding to longer roughness wavelengths), as expected. For instance, the inset shows that the PFA is a good approximation for $L = 50\text{nm}$ and $k < 0.04\text{nm}^{-1}$. On the other hand, for $L = 200\text{nm}$ and $k = 0.02\text{nm}^{-1}$

(roughness wavelength $2\pi/k \simeq 300\text{nm}$) we find $\rho \simeq 1.6$, corresponding to a roughness correction 60% larger than the PFA result.

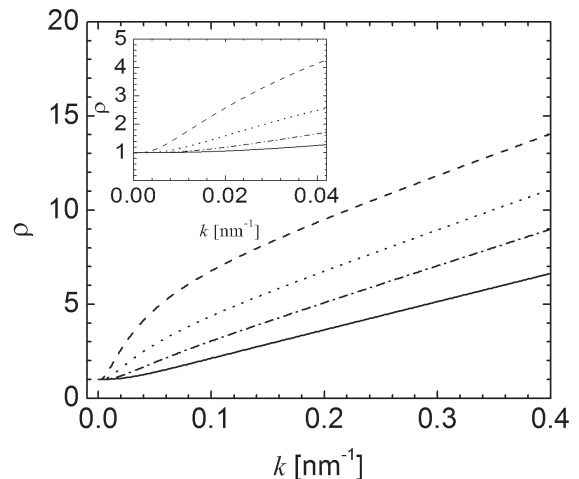


FIG. 4: Variation of ρ versus k for several values of L (same conventions as on Fig. 3).

Fig. 4 also indicates that $\rho(k)$ grows linearly for large values of k . In the next section, we show that this is a general result, valid for arbitrary values of L and λ_{P} .

V. HIGH- k LIMIT

When the momentum transfer k is much larger than $1/L$, the function $b_{\mathbf{k}', \mathbf{k}' - \mathbf{k}}^{(i)}(\xi)$, representing the contribution of the first-order reflection operator, is negligible, because it is proportional to the exponentially small propagation factor $\exp(-\sqrt{(\mathbf{k}' - \mathbf{k})^2 + \xi^2}L) \approx \exp(-kL)$ appearing in Eq. (28). This general property can be understood from the discussion of Sec III: the loop function $\delta f_p^{(2i)}(\mathbf{k}', \xi)$ contains two rough reflections separated by an intracavity round-trip propagation with the modified momentum $\mathbf{k}' - \mathbf{k}$.

On the other hand, the loop function $\delta f_p^{(2ii)}(\mathbf{k}, \xi)$ involves a single second-order rough reflection, which must conserve momentum so as to allow for a closed loop. Thus, $b_{\mathbf{k}', \mathbf{k}' - \mathbf{k}}^{(ii)}$ does not involve propagation with the modified momentum $\mathbf{k}' - \mathbf{k}$ and is the dominant term in the high- k limit. We calculate $b_{\mathbf{k}', \mathbf{k}' - \mathbf{k}}^{(ii)}$ from (40) by taking $\mathbf{k}' - \mathbf{k} \approx -\mathbf{k}$. We also assume that $k \gg k_{\text{P}}$; the opposite case will be discussed in Sec. VI. We find

$$\rho(k) = \alpha k \quad \text{for } k^{-1} \ll \lambda_{\text{P}}, L. \quad (42)$$

The dimensionless parameter α/L depends on $K_{\text{P}} = k_{\text{P}}L = 2\pi L/\lambda_{\text{P}}$ only, and is given by

$$\alpha = \frac{\hbar c A}{(2\pi)^2 L^4 G(0)} \int_0^\infty d\gamma \gamma \int_0^\gamma d\Omega \frac{K_P^2}{2\Omega^2 + K_P^2} \left[\gamma f_{\text{TE}}(\mathbf{k}, \xi) + \frac{2(\gamma^2 - \Omega^2)^2 - \gamma_t^2(2\gamma^2 - 3\Omega^2)}{(\gamma\gamma_t)^2 - (\gamma^2 - \Omega^2)^2} \gamma f_{\text{TM}}(\mathbf{k}, \xi) \right]. \quad (43)$$

We have introduced the dimensionless integration variables $\gamma = \kappa L$, $\gamma_t = \kappa_t L$, and $\Omega = \xi L/c$. $f_{\text{TE}}(\mathbf{k}, \xi)$ and $f_{\text{TM}}(\mathbf{k}, \xi)$ are calculated from (16) as functions of γ and Ω .

We plot the coefficient α as a function of L in Fig. 5, with the plasma wavelength of gold $\lambda_P = 136\text{nm}$ as in the previous numerical examples. At the limit of short distances, we recover from (43) our previous result [11]

$$\alpha = 0.4492L \quad \text{for } k^{-1} \ll L \ll \lambda_P. \quad (44)$$

This corresponds to the high- k limit of the plasmon (non-retarded) regime, which we shall discuss further in Sec. VII. This limit is indicated by the dotted line in Fig. 5.

As shown by Fig. 5, the angular coefficient α saturates at the limit of large distances. This corresponds to the limit $k^{-1} \ll \lambda_P \ll L$, which may be obtained analytically from Eq. (43) by expanding its r.h.s. in powers of λ_P . The integrand vanishes to order λ_P^{-1} , whereas the zero-th order term yields

$$\alpha^{(0)} = - \frac{\hbar c A}{(2\pi)^2 L^4 G(0)} \int_0^\infty d\gamma \frac{1}{e^{2\gamma} - 1} \quad (45)$$

$$\times \int_0^\gamma d\Omega (\gamma^4 - 2\gamma^2\Omega^2 + 3\Omega^4) = 0,$$

so that the dominant term is of the order of λ_P . We also need to calculate $G(0)$ in the limit $L \gg \lambda_P$. As expected, we find $G(0) = E_{\text{PP}}^{\text{pr}}''(L)/2 = -\pi^2 \hbar c A / (120L^5)$, where $E_{\text{PP}}^{\text{pr}}$ is the Casimir energy for perfectly reflecting mirrors. We then find

$$\alpha = \frac{60}{\pi^5} \lambda_P \int_0^\infty d\gamma \frac{e^{2\gamma}}{\gamma(e^{2\gamma} - 1)^2} \quad (46)$$

$$\times \int_0^\gamma d\Omega (\gamma^4 - 2\gamma^2\Omega^2 + 3\Omega^4)$$

giving

$$\alpha = \frac{7}{15\pi} \lambda_P \quad \text{for } k^{-1} \ll \lambda_P \ll L, \quad (47)$$

which is in agreement with the saturation value shown in Fig. 5. This result remarkably differs from the long distance behavior reported in Ref. [11], which corresponds to the perfectly-reflecting limit. Note that the high- k expression (43) holds when the roughness length scale $1/k$ is much smaller than both λ_P and L . In this regime, and as a consequence of the momentum transfer induced by the roughness effect, the modified field momentum has a magnitude $|\mathbf{k}' - \mathbf{k}|$ much larger than k_P . Therefore, it is poorly reflected by the mirrors, even though the initial

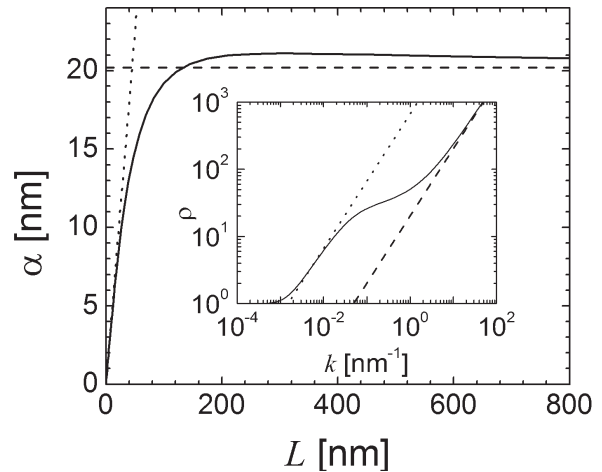


FIG. 5: Variation of the angular coefficient α versus L for $\lambda_P = 136\text{nm}$. The analytical result for $k^{-1} \ll L \ll \lambda_P$ is shown as the dotted line and for $k^{-1} \ll \lambda_P \ll L$ as the dashed line. A comparison between this second result (dashed straight line) and the exact $\rho(k)$ (solid line) is shown in the inset for $L = 2\mu\text{m}$. The analytical result $\rho = Lk/3$ predicted by the model of perfect reflectors (dotted line) is valid only in the intermediate range $\lambda_P \ll k^{-1} \ll L$.

momentum satisfies $k' \lesssim 1/L \ll k_P$. In order to obtain the perfectly-reflecting limit, one must assume that λ_P rather than $1/k$ is the shortest length scale, as discussed in the next section.

VI. PERFECTLY-REFLECTING LIMIT

In this section we assume that λ_P is much smaller than both the separation L and the roughness wavelength $1/k$. Then, we expand $b_{\mathbf{k}', \mathbf{k}''}$ in powers of λ_P . For $b_{\mathbf{k}', \mathbf{k}''}^{(ii)}$, representing the contribution of the second-order reflection operator and given by (40), the dominant term is of the order of $1/\lambda_P$:

$$b_{\mathbf{k}', \mathbf{k}' - \mathbf{k}}^{(ii)} = 4\pi \frac{f^{\text{pr}}(\mathbf{k}')}{\kappa' \lambda_P} \mathbf{k}' \cdot \mathbf{k} + O(\lambda_P^0), \quad (48)$$

where $f^{\text{pr}}(\mathbf{k}')$ represents the loop function for perfect reflectors [it is the same for both polarizations, with $r^{\text{TE}} = -r^{\text{TM}} = -1$, according to (33) and (34)]. On the other hand, $b_{\mathbf{k}', \mathbf{k}' - \mathbf{k}}^{(i)}$ vanishes up to order $1/\lambda_P$. It follows that $G(\mathbf{k})$ vanishes at this order, because when taking the integral of the r.h.s. of (48) over all values of

momentum \mathbf{k}' in (26), opposite values of \mathbf{k}' compensate each other.

Both $b_{\mathbf{k}',\mathbf{k}''}^{(i)}$ and $b_{\mathbf{k}',\mathbf{k}''}^{(ii)}$ contribute up to order λ_P^0 . It is useful to replace $b_{\mathbf{k}',\mathbf{k}''}$ by the symmetrized form

$$\hat{b}_{\mathbf{k}',\mathbf{k}''} = (b_{\mathbf{k}',\mathbf{k}''} + b_{\mathbf{k}'',\mathbf{k}'})/2.$$

This procedure does not change the response function because $G(\mathbf{k}) = G(-\mathbf{k}) = G(k)$. Taking $d^2\mathbf{k}' = dk'k'd\phi'$ in (26), we derive

$$G(\mathbf{k}) = -\frac{\hbar A}{8\pi^3} \int_0^\infty d\xi \int_0^\infty dk'k' \int_0^{2\pi} d\phi' \hat{b}_{\mathbf{k}',\mathbf{k}'-\mathbf{k}}. \quad (49)$$

$\hat{b}_{\mathbf{k}',\mathbf{k}''}$ is obtained from the term of order λ_P^0 in (39) and (40):

$$\hat{b}_{\mathbf{k}',\mathbf{k}''} = \frac{e^{-2\kappa'L} + e^{-2\kappa''L}}{(1 - e^{-2\kappa'L})(1 - e^{-2\kappa''L})} \times \frac{(\kappa'\kappa'')^2 + (\xi^2/c^2 + \mathbf{k}' \cdot \mathbf{k}'')^2}{\kappa'\kappa''}. \quad (50)$$

We change the variables of integration from (ξ, k') to (κ', κ'') . The integral over ϕ' yields

$$\int_0^{\phi_m} |J| k(\kappa', \kappa'', \phi') d\phi' = \frac{\pi \kappa' \kappa''}{2 k}, \quad (51)$$

where $\phi_m = \arcsin[(\kappa'^2 - \kappa''^2 + k^2)/(2\kappa'k)]$ and $|J|$ is the Jacobian corresponding to the transformation.

From (49)–(51) we derive

$$G(k) = -\frac{\hbar c A}{8\pi^2} \frac{1}{L^5 q} \int_0^\infty \frac{d\gamma e^{-2\gamma}}{1 - e^{-2\gamma}} \int_{|\gamma-q|}^{\gamma+q} d\gamma' \times \frac{(\gamma\gamma')^2 + \frac{1}{4}(\gamma^2 + \gamma'^2 - q^2)^2}{1 - e^{-2\gamma'}} \quad \text{for } \lambda_P \rightarrow 0. \quad (52)$$

γ has the same meaning already discussed in connection with (43) while γ' corresponds to the diffracted wave. From (52) we verify that $G(0) = E_{PP}^{pp}/2$ as expected. For arbitrary values of $q = kL$, numerical integration of (52) agrees with the results of Emig *et al.* [21] for a perfectly-reflecting mirror corrugated along a fixed direction in the xy plane. By taking the assumption of perfect reflectivity from the start, we may derive this result for a general deformation directly from our general expressions (26)–(29), as discussed in Appendix C.

In order to discuss the regime $\lambda_P \ll 1/k \ll L$, we now take the high- k limit of the right-hand side of (52). Due to the presence of the exponential factor $\exp(-2\gamma)$, the dominant contribution comes from the corner $\gamma \lesssim 1$, $\gamma' \sim q$ of the rectangle associated to the integration region. We may thus neglect $\exp(-2\gamma')$ and recover the long distance limit of [11]:

$$G(k) = -\frac{2}{3\pi^2} \frac{\hbar c A q}{L^5} \int_0^\infty d\gamma \frac{\gamma^3 e^{-2\gamma}}{1 - e^{-2\gamma}} = -\frac{\pi^2}{360} \hbar A \frac{q}{L^4},$$

$$\rho = \frac{1}{3} L k \quad \text{for } \lambda_P \ll k^{-1} \ll L. \quad (53)$$

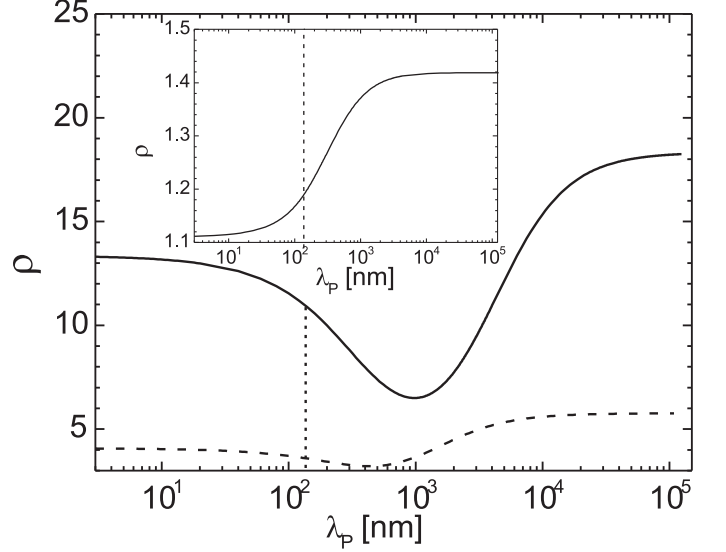


FIG. 6: Variation of ρ versus λ_P for $k = 0.02\text{nm}^{-1}$ and the distances $L = 2\mu\text{m}$ (solid line), $L = 600\text{nm}$ (dashed line) and $L = 100\text{nm}$ (inlet, solid line). The values at $\lambda_P = 136\text{nm}$ are indicated by vertical lines.

In summary, the long-distance behavior is given by (47) when $1/k \ll \lambda_P \ll L$, and by (53) when $\lambda_P \ll 1/k \ll L$. The cross-over between these two regimes is shown in the inlet of Fig. 5, where we plot ρ as a function of k for $L = 2\mu\text{m}$. The finite conductivity of the metals clearly reduces the roughness correction for very large values of kL , due to the saturation effect discussed in Sec. V. In Fig. 6, we plot ρ as function of the plasma wavelength λ_P for $k = 0.02\text{nm}^{-1}$ (roughness wavelength $2\pi/k \approx 300\text{nm}$), with $L = 2\mu\text{m}$ (solid line) and $L = 600\text{nm}$ (dashed line), in order to analyze in detail the effect of finite conductivity. The value $\lambda_P = 136\text{nm}$ corresponding to gold covered mirrors is highlighted by a vertical line. The perfectly-reflecting limit corresponds to the small values of λ_P shown in the left-hand side of the figure. The correction decreases as λ_P approaches $2\pi/k$ because of the saturation effect, and then it increases again as λ_P approaches and goes beyond the separation distance L . For $\lambda_P \gg L$, we find the limit predicted by the plasmon model, to be discussed in the next section, which is larger than the perfectly-reflecting limit [11]. When $kL \lesssim 1$, the correction is always larger than the perfectly-reflecting limit, as illustrated in the inlet of Fig. 6, where we take $k = 0.02\text{nm}^{-1}$ and $L = 100\text{nm}$. In this case, the perfectly-reflecting limit is 11% larger than the PFA result, whereas at $\lambda_P = 136\text{nm}$ we find a correction 19% larger than the PFA.

VII. PLASMON LIMIT

In the short distance regime, $L \ll \lambda_P$, the Casimir energy is associated to surface plasmons. As discussed in the previous sections, when integrating $b_{\mathbf{k}', \mathbf{k}' - \mathbf{k}}$ in (26), the dominant contributions come from values of \mathbf{k}' and ξ such that $\kappa' \lesssim 1/L$. Then, the short-distance limit of (33) yields $r^{\text{TE}} = O(L/\lambda_P)^2$, so that the contribution of TE polarization is negligible. From (34), r^{TM} is also negligible except for the values

$$\xi \lesssim \omega_P \ll c/L, \quad (54)$$

for which $\kappa' \approx k'$, and

$$r^{\text{TM}} \approx \frac{\omega_P^2}{2\xi^2 + \omega_P^2}. \quad (55)$$

In other words, the dominant contribution is associated to low-frequency surface waves, the reflection coefficient having poles at the surface plasmon resonance $\xi = -i\omega_P/\sqrt{2}$. From (54), we also conclude that the retardation time L/c for propagation between the mirrors is negligible in the time scale associated to the relevant field frequencies.

We calculate the roughness correction by taking the appropriate limits in (39) and (40). Since r^{TM} only depends on ξ , the diffracted wave sees the same reflection coefficient, which we denote as r for simplicity. We find

$$b_{\mathbf{k}', \mathbf{k}''}^{(i)} = \frac{k'k'' r^4 e^{-2k'L} e^{-2k''L}}{2(1 - r^2 e^{-2k'L})(1 - r^2 e^{-2k''L})} [(C + 1)^2 + 2r(1 - C^2) + r^2(1 - C^2)^2], \quad (56)$$

$$b_{\mathbf{k}', \mathbf{k}''}^{(ii)} = \frac{2k'^2 r^2 e^{-2k'L}}{1 - r^2 e^{-2k'L}} + \frac{k'k'' r^3 e^{-2k'L}}{1 - r^2 e^{-2k'L}} [r(1 - C)^2 + 1 - C^2]. \quad (57)$$

These equations do not agree with the results of Ref. [10], which in their turn are not consistent with the PFA. Therefore, it is important to check our results against the PFA by taking $k'' = k' = k$ and $C = 1$ in (56) and (57):

$$b_{\mathbf{k}, \mathbf{k}} = \frac{2k^2 r^2 e^{-2kL}}{(1 - r^2 e^{-2kL})^2}. \quad (58)$$

When replacing this result into (26), and taking (55) into account (with $\zeta = \xi/\omega_P$, and $\gamma = \kappa L = kL$), we obtain

$$G(0) = -\frac{\hbar A \omega_P}{2\pi^2 L^4} \int_0^\infty d\zeta \int_0^\infty d\gamma \frac{\gamma^3 (2\zeta^2 + 1) e^{2\gamma}}{[(2\zeta^2 + 1)^2 e^{2\gamma} - 1]^2}$$

Integrating this expression by parts, one shows that $G(0)$ satisfies (31), with E_{PP} representing the short-distance limit of the Casimir energy as given by [22]:

$$E_{\text{PP}}(L) = -\frac{\hbar A \omega_P}{4\pi^2 L^2} \int_0^\infty d\zeta \int_0^\infty d\gamma \frac{\gamma^2}{(2\zeta^2 + 1)^2 e^{2\gamma} - 1}.$$

This confirms consistency with the PFA, which is in line with the more general discussion presented in Appendix B.

In addition to the limit $k \rightarrow 0$, it is also interesting to analyze the case $k \gg 1/L$ from (56) and (57), allowing for the evaluation of the limit $1/k \ll L \ll \lambda_P$. This provides as additional check, by comparison with the results of

Sec. V. In this limit, $b_{\mathbf{k}', \mathbf{k}' - \mathbf{k}}^{(i)}$ is exponentially small, and the dominant contribution for $b_{\mathbf{k}', \mathbf{k}' - \mathbf{k}}^{(ii)}$ comes from the second term in (57), which is proportional to k :

$$b_{\mathbf{k}', \mathbf{k}' - \mathbf{k}} \approx b_{\mathbf{k}', -\mathbf{k}} \approx \frac{k' r^3 e^{-2k'L}}{1 - r^2 e^{-2k'L}} [r(1 - C)^2 + 1 - C^2] k. \quad (59)$$

We also take $C \approx -\mathbf{k}' \cdot \mathbf{k}/(kk') = -\cos \phi$, and integrate over ϕ to derive from (26)

$$G(k) = -\frac{\hbar A \omega_P}{8\pi^2 L^3} k \times \int_0^\infty d\zeta \int_0^\infty d\gamma \frac{\gamma^2 (2\zeta^2 + 4)}{(2\zeta^2 + 1)^2 [(2\zeta^2 + 1)^2 e^{2\gamma} - 1]}, \quad (60)$$

yielding $\rho(k) = 0.4492Lk$, in agreement with Eq. (44) and Ref. [11].

VIII. CONCLUDING REMARKS

We have calculated the second-order response function $G(k)$ for arbitrary values of the plasma wavelength λ_P and the distance L . This allows for a reliable computation of the roughness correction, once the roughness spectrum $\sigma(\mathbf{k})$ characterizing the metallic surfaces is experimentally determined. In order to gain further insight into the roughness correction itself, we consider the

particularly simple example of a Gaussian spectrum [10]:

$$\sigma[\mathbf{k}] = \pi a^2 \ell_C^2 \exp\left(-\frac{\mathbf{k}^2 \ell_C^2}{4}\right). \quad (61)$$

The roughness variance values a^2 , and ℓ_C represents the correlation length.

According to Eq. (25), the relative force correction Δ is obtained by integrating the normalized response function $G(k)/E_{PP}$ (see Fig. 3 for some numerical examples) over the Gaussian spectrum given by (61). In Ref. [14], we have discussed some simple analytical expressions in the limiting cases $\lambda_P \ll \ell_C$ and $\lambda_P \gg \ell_C$, which can be easily derived from the results of Secs. V–VII. However, the experimental parameters are likely to be such that neither of the two limits holds. Hence, we must rely on the numerical calculation of $G(k)$ to compute the correction. In Fig. 7, we compare the exact results for Δ/a^2 (for two different values of ℓ_C) with the PFA formula $\Delta/a^2 = E''_{PP}(L)/[2E_{PP}(L)]$, taking as before $\lambda_P = 136\text{nm}$. At $L = 100\text{nm}$, the exact value is 57% and 7% larger than the PFA result for $\ell_C = 50\text{nm}$ and $\ell_C = 150\text{nm}$, respectively. In agreement with the discussion of Sec. IV, the PFA is better for shorter distances and longer correlation lengths. For instance, as suggested by Fig. 7, it provides accurate results if $L < 100\text{nm}$ and $\ell_C > 150\text{nm}$. Note, however, that the validity of the PFA can be addressed in a reliable way only from the analysis of the experimentally measured roughness spectrum. In the Gaussian model discussed in this section, the contribution of high values of k are exponentially small, but in the real case the decay of $\sigma(k)$ might be smoother. Thus, this approximation might be worse than discussed here.

For large values of L , no simple analytical result is available when $\lambda_P \sim \ell_C$. In the inlet of Fig. 7, we show that the perfectly-reflecting result $\Delta/a^2 = 2\sqrt{\pi}/(\ell_C L)$ valid for $\lambda_P \ll \ell_C \ll L$ overestimates the correction for $\ell_C = 50\text{nm}$ by more than 50%. This is a consequence of the saturation effect discussed in Sec. V: diffraction by roughness Fourier components at $k > \lambda_P^{-1}$ give rise to waves which are poorly reflected by the mirrors. Thus, when the roughness spectrum contains very high values of k , the correction is reduced with respect to the result of the perfectly-reflecting model. The reduction factor decreases as $k\lambda_P \rightarrow \infty$ down to the limit $(7/5\pi)\lambda_P/L \ll 1$.

In conclusion, we presented a perturbative method for the calculation of the Casimir energy between rough mirrors, up to second order in the amplitude of the deformation. It relies on the manipulation of reflection operators, taking into account diffraction and the coupling between different field polarizations. We applied the method to compute the roughness correction in the framework of the plasma model, for arbitrary values of the plasma and roughness wavelengths and the mirror separation L . Analytical results for different limiting cases were discussed. In particular, the PFA regime follows from our formalism in the limit of very smooth surface profiles. By compar-

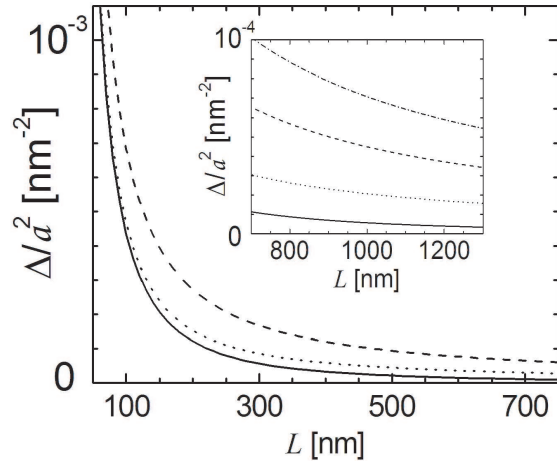


FIG. 7: Roughness correction for the Gaussian spectrum. We plot the relative force correction for the plane-sphere setup over the squared amplitude of roughness, Δ/a^2 , versus L for $\ell_C = 50\text{nm}$ (dashed line) and $\ell_C = 150\text{nm}$ (dotted line). The solid line represents the PFA result. In the inlet, we also plot the long-distance perfectly-reflecting limit (dot-dash). We take $\lambda_P = 136\text{nm}$.

ison with our numerical results, we were able to analyze the accuracy of the PFA in the problem of roughness. For a given roughness spectrum, our theory provides reliable numerical results for the roughness correction, and allows to check the validity of the PFA approach in a given experiment. More realistic models for the metallic mirrors [7] can also be considered by applying the formal results presented here.

We thank Cyriaque Genet and Marc-Thierry Jaekel for discussions. PAMN thanks Instituto do Milênio de Informação Quântica and CNPq for partial financial support.

APPENDIX A: OPTICAL NETWORK THEORY AND THE CASIMIR FORCE

In this appendix, we compute the spectral density in the intracavity region by generalizing the optical network formalism of Ref. [13] to the case of rough surfaces. This allows us to compute the Casimir force with the help of the Maxwell stress tensor.

The basic idea is to derive the relation between the intracavity field and the incoming outside field, whose fluctuations are known. The outside field propagating from the region $z < 0$ (see Fig. 1) is written as [with $\mathbf{r} = (x, y)$, $\omega = c\sqrt{k^2 + k_z^2}$ and ϵ_0 denoting the vacuum

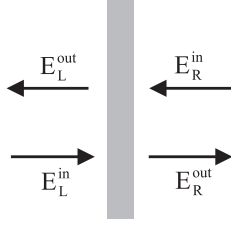


FIG. 8: Input and output fields.

permittivity]

$$\mathbf{E}_L^{\text{in}}(\mathbf{r}, z, t) = \sum_{p=\text{TE}, \text{TM}} \int \frac{d^2\mathbf{k}}{4\pi^2} \int_0^\infty \frac{dk_z}{2\pi} \sqrt{\frac{\hbar\omega}{2\epsilon_0}} e_L^{\text{inp}}(\mathbf{K}) \times \exp[i(\mathbf{k} \cdot \mathbf{r} + k_z z - \omega t)] \hat{e}^p + \text{H.c.} \quad (\text{A1})$$

The Fourier components $e_L^{\text{inp}}(\mathbf{K})$ satisfy the commutation relations of freely-propagating fields:

$$[e_L^{\text{inp}}(\mathbf{K}), e_L^{\text{inp}'}(\mathbf{K}')^\dagger] = (2\pi)^3 \delta^{(2)}(\mathbf{k} - \mathbf{k}') \delta(k_z - k'_z) \delta_{p,p'}. \quad (\text{A2})$$

The free-space fields propagating along the negative z -direction are written in a similar way, except for the replacement $\exp(ik_z z) \rightarrow \exp(-ik_z z)$. We use the same $\mathbf{K} = \mathbf{k} + k_z \hat{z}$ to label them as well, and our notation is such that $k_z > 0$ in all cases.

We define scattering and transfer operators for the two rough mirrors and for the empty-space propagation between them. The cavity is taken as a composed network, and the corresponding transfer operator is simply the product of the transfer operators for the elementary components.

The scattering operator characterizing a given element of the network is defined in the following way. As shown in Fig. 8, the input field contains components propagating from the left and righthanded sides, and with polarizations TE and TM. We arrange these components into

a column vector:

$$\mathbf{e}^{\text{in}}(\mathbf{K}) \equiv \begin{pmatrix} e_L^{\text{inTE}} \\ e_R^{\text{inTE}} \\ e_L^{\text{inTM}} \\ e_R^{\text{inTM}} \end{pmatrix}_{\mathbf{K}}$$

We employ a similar notation for the output field:

$$\mathbf{e}^{\text{out}}(\mathbf{K}) = \begin{pmatrix} e_R^{\text{outTE}} \\ e_L^{\text{outTE}} \\ e_R^{\text{outTM}} \\ e_L^{\text{outTM}} \end{pmatrix}_{\mathbf{K}}$$

The scattering operator provides the input-output relation

$$\mathbf{e}^{\text{out}}(\mathbf{K}) = \int_{(k'_z > 0)} \frac{d^3 K'}{(2\pi)^3} \mathbf{S}(\mathbf{K}, \mathbf{K}') \mathbf{e}^{\text{in}}(\mathbf{K}') \quad (\text{A3})$$

where the integral over k'_z runs from 0 to ∞ .

Whereas Ref. [13] allows for lossy mirrors, here we assume that there is no dissipation in our network. Hence we only consider unitary scattering operators: $\mathbf{S} \cdot \mathbf{S}^\dagger = \mathbf{1}$, where $\mathbf{1}$ is the identity operator. In terms of the corresponding matrix multiplication, this condition reads (\mathbf{I} is the 4×4 identity matrix)

$$\int_{(k'_z > 0)} \frac{d^3 K'}{(2\pi)^3} \mathbf{S}(\mathbf{K}_1, \mathbf{K}') \mathbf{S}(\mathbf{K}_2, \mathbf{K}')^\dagger = (2\pi)^3 \delta^{(3)}(\mathbf{K}_1 - \mathbf{K}_2) \mathbf{I}. \quad (\text{A4})$$

We analyze in detail the scattering operator \mathbf{S}_1 corresponding to mirror M1 in Fig. 1. We expand \mathbf{S}_1 up to second order of the deformation amplitudes of the two lateral mirror's rough surfaces:

$$\mathbf{S}_1 = \mathbf{S}_1^{(0)} + \delta\mathbf{S}_1^{(1)} + \delta\mathbf{S}_1^{(2)}. \quad (\text{A5})$$

The scattering by ideal plane surfaces conserves ω , \mathbf{k} and polarization:

$$\mathbf{S}_1^{(0)}(\mathbf{K}, \mathbf{K}') = (2\pi)^3 \delta^{(3)}(\mathbf{K} - \mathbf{K}') \begin{pmatrix} \tilde{r}_1^{\text{TE}}(\mathbf{k}, \omega) & r_1^{\text{TE}}(\mathbf{k}, \omega) & 0 & 0 \\ \tilde{r}_1^{\text{TE}}(\mathbf{k}, \omega) & t_1^{\text{TE}}(\mathbf{k}, \omega) & 0 & 0 \\ 0 & 0 & \tilde{r}_1^{\text{TM}}(\mathbf{k}, \omega) & r_1^{\text{TM}}(\mathbf{k}, \omega) \\ 0 & 0 & \tilde{r}_1^{\text{TM}}(\mathbf{k}, \omega) & t_1^{\text{TM}}(\mathbf{k}, \omega) \end{pmatrix}.$$

$r_1^p(\mathbf{k}, \omega)$ are the specular reflection coefficients as seen by the intracavity field presented in Sec. III. The coefficients $\tilde{r}_2^p(\mathbf{k}, \omega)$ play the same role for mirror M2. Together they turn out to be the only relevant ones for the calculation of the Casimir effect, both in the ideal and rough cases. For simplicity, we have denoted $\tilde{r}_2^p(\mathbf{k}, \omega)$ simply as $r_2^p(\mathbf{k}, \omega)$ everywhere in this paper, except in the present appendix.

The first ($\ell = 1$) and second-order ($\ell = 2$) corrections mix up different polarizations and values of \mathbf{k} , but conserve

the frequency:

$$\delta \mathbf{S}_1^{(\ell)}(\mathbf{K}, \mathbf{K}') = 2\pi \delta(k'_z - \sqrt{k^2 - k'^2 + k_z^2}) \begin{pmatrix} \delta \tilde{t}_1^{(\ell)}[\text{TE};\text{TE}] & \delta r_1^{(\ell)}[\text{TE};\text{TE}] & \delta \tilde{t}_1^{(\ell)}[\text{TE};\text{TM}] & \delta r_1^{(\ell)}[\text{TE};\text{TM}] \\ \delta \tilde{r}_1^{(\ell)}[\text{TE};\text{TE}] & \delta t_1^{(\ell)}[\text{TE};\text{TE}] & \delta \tilde{r}_1^{(\ell)}[\text{TE};\text{TM}] & \delta t_1^{(\ell)}[\text{TE};\text{TM}] \\ \delta \tilde{t}_1^{(\ell)}[\text{TM};\text{TE}] & \delta r_1^{(\ell)}[\text{TM};\text{TE}] & \delta \tilde{t}_1^{(\ell)}[\text{TM};\text{TM}] & \delta r_1^{(\ell)}[\text{TM};\text{TM}] \\ \delta \tilde{r}_1^{(\ell)}[\text{TM};\text{TE}] & \delta t_1^{(\ell)}[\text{TM};\text{TE}] & \delta \tilde{r}_1^{(\ell)}[\text{TM};\text{TM}] & \delta t_1^{(\ell)}[\text{TM};\text{TM}] \end{pmatrix} \quad (\text{A6})$$

All matrix elements above are functions of frequency and of the initial and final momenta \mathbf{k}' and \mathbf{k} . The four elements $\delta r_1^{(\ell)}[p; p']$ are the matrix elements $\langle \mathbf{k}, p | \delta \mathcal{R}_1^{(\ell)} | \mathbf{k}', p' \rangle$ introduced in Sec. III.

The transfer operators \mathbf{T} provide the fields at the left-hand side of the mirror in terms of the fields at the right-hand side. They can be obtained from the scattering operators as follows [13]:

$$\mathbf{T} = -(\mathbf{P}_- - \mathbf{S} \cdot \mathbf{P}_+)^{-1} \cdot (\mathbf{P}_+ - \mathbf{S} \cdot \mathbf{P}_-). \quad (\text{A7})$$

The operators \mathbf{P}_+ and \mathbf{P}_- are defined by

$$\mathbf{P}_+(\mathbf{K}, \mathbf{K}') = (2\pi)^3 \delta^3(\mathbf{K} - \mathbf{K}') \begin{pmatrix} 1 & 0 & 0 & 0 \\ 0 & 0 & 0 & 0 \\ 0 & 0 & 1 & 0 \\ 0 & 0 & 0 & 0 \end{pmatrix},$$

$$\mathbf{P}_- = \mathbf{1} - \mathbf{P}_+.$$

The intracavity field (see Fig. 1)

$$\mathbf{e}^C(\mathbf{K}) = \begin{pmatrix} \rightarrow_{\text{C}}^{\text{TE}} \\ e_{\text{C}} \\ \leftarrow_{\text{C}}^{\text{TE}} \\ \rightarrow_{\text{C}}^{\text{TM}} \\ e_{\text{C}} \\ \leftarrow_{\text{C}}^{\text{TM}} \\ e_{\text{C}} \end{pmatrix}_{\mathbf{K}}$$

is computed from

$$\mathbf{e}^C(\mathbf{K}) = \int_{(k'_z > 0)} \frac{d^3 K'}{(2\pi)^3} \mathbf{R}(\mathbf{K}, \mathbf{K}') \mathbf{e}^{\text{in}}(\mathbf{K}'), \quad (\text{A8})$$

with

$$\mathbf{R} = \mathbf{T}_2 \cdot \mathbf{P}_+ \cdot \mathbf{S}_{\text{cav}} + \mathbf{T}_2 \cdot \mathbf{P}_-, \quad (\text{A9})$$

and where \mathbf{S}_{cav} is the scattering matrix for the cavity as a composed network.

The Casimir force on mirror M1 is computed from the energy-momentum tensor component T_{zz} , evaluated at the intracavity region and at the outer side of the mirror, and averaged over the vacuum state:

$$F_{\text{PP}} = \int d^2 r [\langle T_{zz}^{\text{L}}(\mathbf{r}) \rangle_{\text{vac}} - \langle T_{zz}^{\text{C}}(\mathbf{r}) \rangle_{\text{vac}}]. \quad (\text{A10})$$

We calculate $T_{zz}^{\text{L}}(\mathbf{r})$ using Eq. (A1) and similar expansions for the magnetic field $\mathbf{B}_{\text{L}}^{\text{in}}$ and for the outgoing fields:

$$\int d^2 r \langle T_{zz}^{\text{L}}(\mathbf{r}) \rangle_{\text{vac}} = \frac{1}{2} \int_{(k_z > 0)} \frac{d^3 K}{(2\pi)^3} \int_0^\infty \frac{dk'_z}{2\pi} \hbar \omega \cos^2 \theta \sum_p \langle [e_{\text{L}}^{\text{inp}}(\mathbf{k}, k_z) e_{\text{L}}^{\text{inp}}(\mathbf{k}, k'_z)^\dagger + e_{\text{L}}^{\text{outp}}(\mathbf{k}, k_z) e_{\text{L}}^{\text{outp}}(\mathbf{k}, k'_z)^\dagger] \rangle_{\text{vac}}, \quad (\text{A11})$$

with $\cos \theta = k_z/K$. A similar expression is found for the inner region in terms of the intracavity fields.

When taking the average over the vacuum state we use the commutation relation (A2) to find

$$\langle e_{\text{L}}^{\text{inp}}(\mathbf{k}, k_z) e_{\text{L}}^{\text{inp}}(\mathbf{k}, k'_z)^\dagger \rangle_{\text{vac}} = 2\pi A \delta(k_z - k'_z). \quad (\text{A12})$$

The outgoing field $e_{\text{L}}^{\text{out}}$ satisfies the same commutation relation, and provides an identical contribution in Eq. (A11).

On the other hand, the commutation relation of the

intracavity field is modified by the joint effect of the two mirrors. We derive the corresponding spectral density from Eqs. (A8), (A9) and (A12):

$$\langle \vec{e}_{\text{C}}^p(\mathbf{k}, k_z) \vec{e}_{\text{C}}^p(\mathbf{k}, k'_z)^\dagger \rangle_{\text{vac}} = 2\pi A g_p(\mathbf{k}, \omega) \delta(k_z - k'_z), \quad (\text{A13})$$

We obtain the explicit expressions for $\delta f_p^{(\text{2ii})}(\mathbf{k}, \omega)$ and $\delta f_p^{(\text{2i})}(\mathbf{k}, \omega)$ given by Eqs. (19) and (23) with the help of a computer algebra system. Remarkably, they only contain the rough reflection coefficients associated to in-

ternal reflections [only 4 out of 16 elements in Eq. (A6) for instance].

The spectral density for $\overleftarrow{\epsilon}_C$ is modified, with respect to the free-space case, by the same generalized Airy function $g_p(\mathbf{k}, \omega)$, as far as second order terms containing rough reflections at the *same* mirror are concerned. After replacing (A12) into (A11), and using (A10) and (A13), we derive the result given by Eq. (14) for the Casimir force.

APPENDIX B: PROXIMITY FORCE APPROXIMATION AS A LIMITING CASE

In this appendix, we derive the PFA result for the energy correction as a limiting case of the general results of Sec. III. This will bring a deeper understanding of the PFA, by showing its connection with some specific properties of the reflection operators. These properties must be satisfied regardless of the particular model considered for the material medium, and are related to the specular reflection by displaced plane mirrors (specular limit).

In the PFA regime, the Fourier profile functions $H_j(\Delta\mathbf{k})$ are sharply peaked around $\Delta\mathbf{k} = \mathbf{0}$. Thus, we may replace \mathbf{k}' by \mathbf{k} in the argument of the non-specular coefficients appearing in the r.-h.-s. of (20) and (21). The resulting expressions correspond to the case of ideal plane mirrors which are displaced from the associated reference planes at $z = 0$ and $z = L$. In this case, the reflection is modified with respect to the non-perturbed case just by the effect of the propagation from the reference plane to the mirror and back. Up to second order, this amounts to take the series expansion of the exponential factor

$$e^{-2\kappa h_j} \approx 1 - 2\kappa h_j + 2\kappa^2 h_j^2,$$

yielding

$$R_{j;pp'}^{(1)}(\mathbf{k}, \mathbf{k}; \xi) = -2\kappa r_j^p(\mathbf{k}, \xi) \delta_{p,p'} \quad (\text{B1})$$

and

$$R_{j;p}^{(2)}(\mathbf{k}, \mathbf{k}; \xi) = 2\kappa^2 r_j^p(\mathbf{k}, \xi). \quad (\text{B2})$$

Eqs. (B1) and (B2) are general properties of the reflection coefficients, and are useful for checking explicit calculations, regardless of the specific model considered for the material medium. When using these results to compute $G(\mathbf{0})$ from Eqs. (26)-(29), we obtain Eq. (31), with the Casimir energy in the ideal case given by (32). This verifies the PFA limit as discussed in the end of Sec. III.

APPENDIX C: PERFECT MIRRORS

In Sec. V, the perfectly-reflecting limit was derived from the plasma model results by taking $\lambda_p \ll k^{-1}, L$.

This appendix presents an alternative, simpler derivation, in which the usual model of perfect reflectors is taken from the start. The case of corrugation along a fixed direction in the xy plane (say the direction along the x -axis, with $h_1(x, y) = h_1(x)$) was considered by Ref. [21]. In this case, the calculation can be considerably simplified by taking a convenient definition for the field polarizations, which then turn out to be not coupled by the scattering from the surface. On the other hand, in this paper we consider arbitrary small-amplitude deformations, so that the coupling between different polarizations has to be taken into account.

For the mirror near $z = 0$, we take the boundary condition

$$\hat{n}_1(x, y) \times \mathbf{E}(x, y, h_1(x, y)) = \mathbf{0}, \quad (\text{C1})$$

where $\hat{n}_1(x, y)$ is the unitary vector normal to the tangent plane at the point (x, y) :

$$\hat{n}_1(x, y) = \frac{\hat{z} - \nabla h_1}{\sqrt{1 + (\nabla h_1)^2}}.$$

As explained in Sec. II, positive values of $h_1(x, y)$ are defined along the positive z axis, and the (intracavity) incident field, as given by (7) propagates along the negative z axis with a phase factor $e^{-ik_z z}$.

Solving (C1) up to first order of $h_1(x, y)$, we determine the complete first-order reflection operator. Using the matrix notation introduced in Sec. IV, the first-order non-specular coefficients defined by Eq. (21) are written as

$$\mathbf{R}^{(1)}(\mathbf{k}, \mathbf{k}'; \omega) = 2i \begin{pmatrix} k'_z C & \omega S/c \\ \frac{\omega k'_z}{ck_z} S & \frac{k k'}{k_z} - \frac{\omega^2}{ck_z} C \end{pmatrix}, \quad (\text{C2})$$

where C and S are the cosine and sine of the angle between \mathbf{k} and \mathbf{k}' .

We only need the diagonal elements of the second-order reflection operator, which we collect from the solution of (C1) up to second order. The corresponding non-specular coefficients [see Eq. (20)] are

$$R_{\text{TE}}^{(2)}(\mathbf{k}, \mathbf{k}'; \omega) = 2k_z k'_z C^2 + 2 \frac{\omega^2 k_z}{c^2 k'_z} S^2 \quad (\text{C3})$$

$$R_{\text{TM}}^{(2)}(\mathbf{k}, \mathbf{k}'; \omega) = -\frac{2}{k_z k'_z} (k k' - \omega^2 C/c^2)^2 - 2 \frac{\omega^2 k'_z}{c^2 k_z} S^2 \quad (\text{C4})$$

These results satisfy the specular limit discussed in Appendix B. When replaced into the general expressions of Sec. III, they reproduce the results for the perfectly-reflecting limit of Sec. V.

-
- [1] H.B.G. Casimir, Proc. K. Ned. Akad. Wet. B **51** 793 (1948).
- [2] S.K. Lamoreaux, Phys. Rev. Lett. **78** 5 (1997); U. Mohideen and A. Roy, *ibid.* **81** 4549 (1998); B.W. Harris, F. Chen and U. Mohideen, Phys. Rev. A **62** 052109 (2000); Th. Ederth, *ibid.* **A 62** 062104 (2000); H.B. Chan, V.A. Aksyuk, R.N. Kleiman, D.J. Bishop and F. Capasso, Science **291** 1941 (2001); G. Bressi, G. Carugno, R. Onofrio and G. Ruoso, Phys. Rev. Lett. **88** 041804 (2002); R.S. Decca, D. López, E. Fischbach and D. E. Krause, *ibid.* **91** 050402 (2003); R.S. Decca, D. López, E. Fischbach, G.L. Klimchitskaya, D. E. Krause and V.M. Mostepanenko, arXiv:quant-ph/0503105 (2005).
- [3] M. Bordag, U. Mohideen and V.M. Mostepanenko, Phys. Reports **353** 1 (2001); A. Lambrecht and S. Reynaud, Séminaire Poincaré **1** 107 (2002); F. Chen, G.L. Klimchitskaya, U. Mohideen and V.M. Mostepanenko, Phys. Rev. A **69** 022117 (2004).
- [4] R.S. Decca, E. Fischbach, G.L. Klimchitskaya, D.E. Krause, D. Lopez and V.M. Mostepanenko Phys. Rev. D **68** 116003 (2003).
- [5] C. Genet, A. Lambrecht and S. Reynaud, Phys. Rev. A **62** 012110 (2000); M. Boström and Bo E. Sernelius, Phys. Rev. Lett. **84**, 4757 (2000); V.B. Svetovoy and M.V. Lokhanin, Mod. Phys. Lett. A **15**, 1013 and 1437 (2000); Phys. Lett. A **280**, 177 (2001); M. Bordag, B. Geyer, G.L. Klimchitskaya and V.M. Mostepanenko, Phys. Rev. Lett. **85**, 503 (2000); G.L. Klimchitskaya and V.M. Mostepanenko, Phys. Rev. A **63**, 062108 (2001); V.B. Bezerra, G.L. Klimchitskaya and V.M. Mostepanenko, Phys. Rev. A **65**, 052113 (2002); J.R. Torgerson and S.K. Lamoreaux, Phys. Rev. E **70**, 047102 (2004); I. Brevik, J.B. Aarseth, J.S. Hoye, and K.A. Milton, Phys. Rev. E **71**, 056101 (2005).
- [6] J. Heinrichs, Phys. Rev. B **11**, 3625 (1975); S.K. Lamoreaux, Phys. Rev. A **59**, R3149 (1999); G.L. Klimchitskaya, U. Mohideen and V.M. Mostepanenko, Phys. Rev. A **61**, 062107 (2000).
- [7] A. Lambrecht and S. Reynaud, Eur. Phys. J. D **8**, 309 (2000).
- [8] J. van Bree, J. Poulis, B. Verhaar and K. Schram, Physica **78**, 187 (1974); M. Bordag, G.L. Klimchitskaya and V.M. Mostepanenko, Phys. Lett. A **200**, 95 (1995).
- [9] G.L. Klimchitskaya, A. Roy, U. Mohideen and V.M. Mostepanenko, Phys. Rev. A **60**, 3487 (1999).
- [10] A.A. Maradudin and P. Mazur, Phys. Rev. B **22** 1677 (1980); P. Mazur and A.A. Maradudin, *ibid.* **B 23** 695 (1981).
- [11] C. Genet, A. Lambrecht, P.A. Maia Neto and S. Reynaud, Europhys. Lett. **62** 484 (2003).
- [12] B.V. Deriagin, I.I. Abrikosova and E.M. Lifshitz, Quart. Rev. **10** 295 (1968).
- [13] C. Genet, A. Lambrecht and S. Reynaud, Phys. Rev. A **67**, 043811 (2003).
- [14] P.A. Maia Neto, A. Lambrecht and S. Reynaud, Europhys. Lett. **69**, 924 (2005).
- [15] D. Langbein, J. Phys. Chem. Solids **32**, 1657 (1971); J.E. Kiefer et al., J. Colloid and Interface Sci. **67**, 140 (1978); R. Balian and B. Duplantier, Annals of Phys. **112**, 165 (1978).
- [16] B.W. Harris, F. Chen, and U. Mohideen, Phys. Rev. A **62**, 052109 (2000).
- [17] M.T. Jaekel and S. Reynaud, J. Physique I-1, 1395 (1991); also available as arXiv:quant-ph/0101067.
- [18] Note that the matrix elements of the reflection operators have dimension of area, as can be checked from Eq. (11), so that the loop function as given by (19) is dimensionless. Moreover, the diagonal elements given by (20) are actually proportional to A because of Eq. (3). Hence the loop function is independent of A as expected.
- [19] J.-J. Greffet, Phys. Rev. B **37** 6436 (1988).
- [20] G.S. Agarwal, Phys. Rev. B **15** 2371 (1977).
- [21] T. Emig, A. Hanke, R. Golestanian and M. Kardar, Phys. Rev. Lett. **87**, 260402 (2001); Phys. Rev. A **67**, 022114 (2003).
- [22] N.G. Van Kampen, B.R.A. Nijboer and K. Schram, Phys. Lett. A **26**, 307 (1968).